Characterization of Internal Formaldehyde Production within The Pandora Spectrometer Instrument

Nash Kocur

Thesis submitted to the Faculty of the
Virginia Polytechnic Institute and State University
in partial fulfillment of the requirements for the degree of

Master of Science
in
Electrical Engineering

Elena S. Lind, Chair
Yizheng Zhu
Scott M. Bailey

December 16, 2020
Blacksburg, Virginia

Keywords: DOAS, HCHO, KORUS-AQ

Characterization of Internal Formaldehyde Production within The Pandora Spectrometer Instrument

Nash Kocur

(ABSTRACT)

Formaldehyde (HCHO), plays an important role in atmospheric chemistry and is an indicator of atmospheric oxidation capacity and surface ozone photo chemistry. The Pandora Spectrometer Instruments are deployed within the NASA/ESA sponsored Pandonia Global Network designed for satellite validation of various gases in atmosphere (e.g. ozone, nitrogen dioxide and formaldehyde). In addition, Pandoras are extensively used during national (e.g. DISCOVER-AQ, OWLETS, LISTOS) and international (CINDI, KORUS-AQ) field campaigns organized to better characterise air pollution and its distribution. Recently it was discovered and shown in prior research conducted by (Spinei et al. 2020), that Pandora measurements of atmospheric HCHO are impacted by HCHO produced within the telescope assembly due to temperature dependent off-gassing from the Delrin® plastic components [22]. The purpose of the research covered in this thesis is to provide a methodology to correct total HCHO vertical column densities measured during the past field campaigns. The methodology developed through the course of this thesis is first tested on the Pandora simulated measurements derived from the surface concentration HCHO observations during KORUS-AQ (2016) field campaign. The derived correction using synthetic data shows that the proposed methodology is accurate within 30%. The second part of the thesis characterizes heat transfer processes within the telescope assembly to estimate internal temperature as a function of ambient meteorological conditions. Considering that the Pandora instruments have mostly identical design of their telescope assemblies heat transfer coefficients derived

from one pandora are expected to be applicable to all Pandoras. Convective heat transfer coefficients were derived at VT wind tunnel as a function of wind speed and telescope assembly position. Internally generated power was measured for several different instruments and averaged at 2.15 ± 0.38 W. Total long wave emissivity was calculated at 0.63. Surface absorptivities were estimated from the material properties. Semi-empirically derived model is proposed to estimate the internal temperature based on the heat transfer parameters, ambient temperature, relative humidity, solar flux, wind speed and wind direction. The correlation between the estimated and measured internal temperatures is 0.93 (R^2). Finally, the methodology is applied to the actual HCHO data collected during the KORUS-AQ campaign and the results are compared to concurrent in-situ measurements made aboard DC-8 aircraft for eight days in the months of May and June 2016.

Characterization of Internal Formaldehyde Production within The Pandora Spectrometer Instrument

Nash Kocur

(GENERAL AUDIENCE ABSTRACT)

Formaldehyde (HCHO), is a key indicator of atmospheric health and because of this, it is an important topic for study. The Pandora Sun Photometer is a low cost instrument developed at NASA Goddard Space Flight center. It has been used in the study of HCHO in various field campaigns. During the Korea-United States Air Quality Study (KORUS-AQ), the Long Island Sound Tropospheric Ozone Study (LISTOS) and the Ozone Water-Land Environmental Transition Study (OWLETS) the Pandora instrument design included a component manufactured from Delrin® plastic. It has recently been found to produce HCHO relative to the change in temperature. Due to the location of this component inside the telescope assembly of the Pandora instrument, the HCHO produced by the plastic was incorporated into the data invalidating the results. The purpose of this thesis is to provide a methodology for analyzing this issue through quantification of the HCHO produced by the plastic. An analysis is conducted to provide the ability to quantify the temperature internal to the telescope assembly. In addition, three methods are discussed for applying this to then quantify the proportion of HCHO that had been added to the measurements. Finally, the methods are applied to data collected during the KORUS-AQ campaign and the results are compared to a reliable set of data performed by a different instrument showing the improved agreement on eight days in the months of May and June.

Dedication

I dedicate this thesis to my family who have supported me through my endeavors.

Acknowledgments

I would like to thank my advisor Elena Lind for guidance and tutelage during this research. I would also like to thank my committee members Yizheng Zhu and Scott Bailey. In addition, I would like to thank Dr. Thomas Diller for his help with heat flux sensors, as well as, Dr. Aurelien Borgoltz and the AOE department for use of their wind tunnel. Finally, I would like to thank my mentors Adam Ben Shabat and Victor Stewart.

Contents

List of Figures

List of Abbreviations

DOAS Differential Optical Absorption Spectroscopy

DS Direct Sun

DSC Differential Slant Column

EPA Environmental Protection Agency

ESA European Space Agency

FTIR Fourier-Transform Infrared

HAP Hazardous Air Pollutants

HCHO Formaldehyde

KORUS-AQ Korea-United States Air Quality Study

LISTOS Long Island Sound Tropospheric Ozone Study

NASA National Aeronautics and Space Administration

NESCAUM Northeast States for Coordinated Air Use Management

NOAA National Oceanic and Atmospheric Administration

OH Hydroxl Radical

OWLETS Ozone Water-Land Environmental Transition Study

POM Polyoxymethylene

RMS Root-Mean Squared

RTS Resistance Temperature Detector

TROPOMI Tropospheric Monitoring Instrument

UV Ultra Violet

VOC Volatile Organic Compound

Chapter 1

Thesis objectives and Organization

1.1 Thesis goal and objectives

The main goal of this study is to expand availability of formaldehyde (HCHO) vertical column densities measured by ground-based Pandora spectroscopic instruments during various field campaigns from 2016 to 2019 (KORUS-AQ, OWLETS-2017, 2018, LISTOS-2018). The measurements were impacted by the temperature dependent HCHO generation inside the telescope assembly of the Pandora instruments, exposed to ambient atmospheric conditions [22].

The objectives of this study include:

1. Propose and evaluate methodology to estimate internal to Pandora HCHO production amplitude knowing telescope assembly temperature and simulated Pandora differential slant column density measurements;

2. Propose and evaluate methodology to estimate internal temperature inside a Pandora telescope assembly using real measurements;

3. Apply the proposed methodologies to correct Pandora spectrometer HCHO measurements during the KORUS-AQ (2016) field campaign. The KORUS-AQ field campaign included NASA DC-8 aircraft in situ measurements of vertical HCHO distribution around the Pandora measurement sites. The integrated columns represent a unique opportunity to verify the proposed ground-based data correction.

1.2 Thesis organization

This thesis is organized in the following chapters:

Chapter 2 describes the importance of HCHO and its atmospheric measurements; the techniques commonly used for such measurements and specifically differential optical absorption spectroscopy (applied in this study).

Chapter 3 describes the Pandora spectrometer instrument, the Pandonia Global Network that deploys the Pandora instruments, and Pandora instrument participation in intergovernmental field campaigns from 2016 to 2019.

Chapter 4 describes the use of polyoxymethylene plastic (POM) in the Pandora telescope assembly and characterization of HCHO emission from POM due to temperature. Two parameters are needed to estimate HCHO generation in the telescope assembly: exponential amplitude and internal temperature

Chapter 5 presents three-step methodology to estimate HCHO production exponential amplitude inside the Pandora telescope assembly. The methodology is evaluated using simulated Pandora measurements.

Chapter 6 presents estimation of the internal telescope assembly temperature using heat transfer coefficient measurements.

Chapter 7 presents application of the proposed methodology to correct actual Pandora HCHO measurements collected during the CORUS-AQ field campaign.

Chapter 8 discusses the results.

Chapter 9 presents conclusions.

Chapter 2

Introduction

2.1 Formaldehyde importance

2.1.1 Atmospheric

HCHO is the most abundant carbonyl in the atmosphere. It can be directly emitted into the atmosphere by the industrial processes as well as incomplete combustion of biomass and fossil fuels. Most of it, however, is photo-chemically produced in the atmosphere by the oxidation of methane and non-methane volatile organic compounds of natural and anthropogenic origin. HCHO participates in radical production (e.g. OH) and surface ozone photochemistry [11, 13]. HCHO is also widely used in industry to manufacture "fertilizers, dyes, disinfectants, germicides, embalming fluids, nonfood preservatives, plastics, wood products, and insulating materials" [6]. It has a short life time (few hours), and serves as a proxy for non-methane volatile organic compounds and atmospheric reactivity leading to the production of ozone and secondary organic aerosols [13]. Ozone and aerosols in their turn are toxic to human health and are classified as Criteria Air Pollutants by U.S. EPA. Ambient concentrations of HCHO in urban environments range from less than 1 $\mu g/m^3$ to over 20 $\mu g/m^3$ [3] Because HCHO is produced as a result of ozone photochemistry ambient concentrations have seasonal variation with the largest during summer months and the lowest during winter months.

2.1.2 Health

Inhaled HCHO is of particular concern as it has toxic effects in both humans and animals and is linked to various cancers such as leukaemia and nasopharyngeal cancer. In addition, associations have been made to cancer of the oral cavity, oro- and hypopharynx, pancreas, larynx, lungs and brain as well [1]. Of the 187 hazardous air pollutants (HAP) identified by the EPA, HCHO can be considered the most important as it accounts for more than 50 percent of the cancer risks associated with HAPs. Because of wide usage of HCHO in manufacturing building materials and furniture indoor HCHO concentrations can be significantly higher than outdoors ranging from 12 $\mu g/m^3$ to over 100 $\mu g/m^3$ [3].

2.2 Formaldehyde measurement techniques

Several different measurement techniques are currently utilized for the detection of HCHO present in the atmosphere. The most common of which being Spectroscopic, Chromatographic, and Fluorimetric, noting that while chromatogrphic and fluorimetric both extract samples from the air, remote sensing spectroscopic measurements are non destructive taking measurements without disturbing the medium in which it measures [9]. Currently, through utilization of these techniques, satellite data are validated with aircraft in-situ measurements [15, 27, 28], MAX-DOAS (multi-axis differential optical absorption spectroscopy) from ground positions [8, 26], from on board ship locations [17, 24], as well as, FTIR (Fourier-transform infrared) measurements [11, 25].

A study done in 2005 by Hak et al. [9] performs an intercomparision of several current measurement techniques of atmospheric HCHO. Eight instruments were used from six independent research groups using Differential Absorption Spectroscopy (DOAS), Fourier Transform Infra Red (FTIR) interferometry, the flourimetic Hantzch reaction technique and a chromatographic technique using C18-DNPH-cartridges [9].

The Hantzch fluorimetric technique is based on sensitive wet chemical fluorimetric detection of CH_2O [9]. This technique requires that HCHO is transferred from gas to liquid state and is based on the "Hantzsch" reaction described by Nash [16]. This method is highly selective for HCHO [9].

"In Fourier-Transform Infra Red (FTIR) interferometry, the absorption of infrared light by various molecules is quantified in the wavelength region between 2 and 15 μ meters" [9]. FTIR measurements are commonly used to provide measurements of atmospheric HCHO as well as other atmospheric constituents such as CO, CO^2, NO and various hydrocarbons. The FTIR method of measurement is a non-destructive, spectroscopic technique that involves the passing of an infrared beam through a sample cell or atmosphere. Different wavelengths that are passed through the sample volume are absorbed by it's constituents and the attenuation is subsequently measured by the instrument. HCHO, for example, can be distinguished through its characteristic absorption at 2782 cm^{-1} and 2843 cm^{-1} [11].

2.2.1 Differential Optical Absorption Spectroscopy (DOAS)

DOAS is a spectroscopic remote sensing technique that has widely been used to make measurements of HCHO and the major focus of this study. Passive DOAS is based on radiance/irradiance measurements of solar radiation to retrieve trace gases absorbing along the photon path [20]. Similar to FTIR, this technique relies on the structured and unique nature of molecular absorption cross section patterns of trace gases. The DOAS technique is based upon the modified Beer-Lambert Law which describes the spectral attenuation of electromagnetic radiation by scattering and absorption. As electromagnetic radiation propagates through the atmosphere it interacts with the atmospheric constituents leaving a distinct pattern of attenuation on the spectra of the radiation specific for each constituent present. Due to the unique attenuation structure present in molecular absorption cross-sections, it is

possible to separate molecular absorption from molecular scattering and aerosol extinction [20]. Solar radiation can be used to measure HCHO distributed through the lower part of atmosphere. Hyperspectral measurements of solar irradiance (non-scattered solar photons) are analysed using DOAS in 3 steps: 1) DOAS fitting of optical depth for each trace gas resulting in differential slant column density (number of molecules per cm^2 along the average photon path) relative to the amount in the reference spectrum; 2) estimation of the amount in the reference spectrum and 3) conversion of the total slant column density to the vertical column density using air mass factor.

Equation 2.1 depicts the DOAS principle where the differential absorption by all the gases absorbing at the specified wavelength region is separated from the broadband extinction:

$$\ln \frac{I_o(\lambda, \mu^{ref})}{I(\lambda - \Delta\lambda, \mu) - offset(\lambda)} = \sum_{i=1}^{i=N} \sigma(\lambda, T)_i \cdot \Delta S_i + (\tau_{aero} + \tau_{rayleigh}) \tag{2.1}$$

Where, $I(\lambda)$ is the measured attenuated solar intensity with wavelength λ and potential wavelength shift $\Delta\lambda$ as well as observation geometry μ. $I_o(\lambda)$ is measured reference solar intensity at λ with observation geometry μ^{ref}. $\tau(\lambda, T)$ represents absorption optical depth caused by gas i absorption at λ and effective temperature T along the average photon path. DOAS fit estimates differential slant column densities of each gas along the average photon path relative to slant column density in the reference geometry ($\Delta S_i = S_i - S_i^{ref}$). Figure 2.1 shows uniqueness of the molecular absorption cross sections of several gases present in the atmosphere that allows for their separation.

Total vertical columns from direct sun measurements (C^{total}) are derived from Eq. 2.2 where observation geometry μ is defined by solar zenith angle.

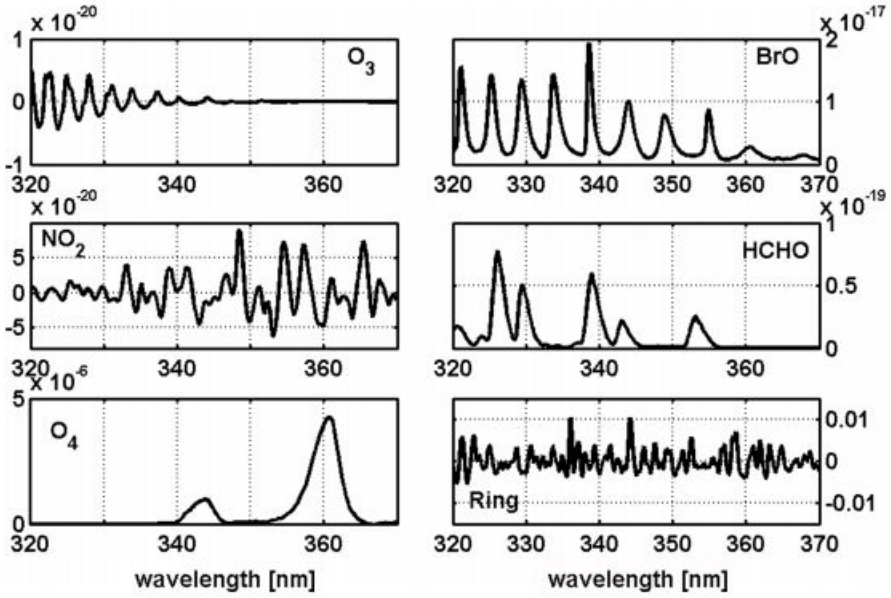

Figure 2.1: Molecular absorption cross sections of trace gases absorbing in the 320–370 nm wavelength range [19].

$$C^{total}(t) = \frac{\Delta S(\lambda,\mu) + S^{ref}(\lambda,\mu^{ref})}{AMF(\mu)} = \left[\frac{molecules}{cm^2}\right] \tag{2.2}$$

$S^{ref}(\lambda,\mu^{ref})$ can be estimated from direct sun measurements using Minimum Langley Extrapolation method (MLE, Herman et al., 2009, see Eq. (2.3)). Where the slope of the smallest ΔS in each ΔAMF bin versus ΔAMF is determined to approximate vertical column at the reference time (C^{ref})):

$$\Delta S(\lambda,\mu) = \underbrace{\Delta C(t)}_{C(t)-C^{ref}(t^{ref})} \cdot AMF(\mu) + C^{ref}(t^{ref}) \cdot \underbrace{\Delta AMF(\mu)}_{AMF(\mu)-AMF^{ref}(\mu^{ref})} \tag{2.3}$$

MLE is a statistical method that relies on availability of long-term measurements. The main assumption being that there are time periods at each solar zenith angle (μ) when $C = C^{ref}(\Delta C = 0)$, and the change in smallest ΔS at each ΔAMF bin is only caused by the change in AMF. This assumption, however, might not be valid for photo chemically produced gases such as HCHO.

Chapter 3

Pandonia Global Network and Pandora instruments

3.1 Pandonia Global Network

In an effort to provide systematic processing and dissemination of data focused on air quality and atmospheric composition, NASA and ESA are funding the ground-based Pandonia Global Network [5]. The network consists of standardized, well calibrated, fully autonomous Pandora instruments [10]. The network was launched in 2019 in order to establish long-term fixed locations to provide high quality observations of total column and vertically resolved concentrations of various trace gases (e.g. NO_2, $HCHO$, SO_2, O_3). The Pandonia Global Network seeks to support the validation of more than a dozen low-earth and geostationary orbit satellites making UV-visible measurements as well as " to coordinate and implement network standards regarding common algorithms and data processing, instrument operating routines, quality control, real-time data processing, and data archiving" [10].

3.2 Pandora instrument

The Pandora project started at NASA Goddard Space Flight Center by Jay Herman, Alexander Cede and Nader Abuhassan in order to address the gap in air quality satellite validation measurements. Pandora system is a cost effective, easy to deploy, compact ground-based spectrometer instrument providing high quality UV/visible measurements using direct

sun/lunar irradiance or sky radiance [10]. Each Pandora instrument is centrally calibrated and has been continually improved. Pandora operation and data processing is based on the DOAS principle and capable of all DOAS observation geometries including direct sun (total trace gas columns), multi-axis (vertical profiles within the lowest 2-3 km), direct moon (total columns)

The instrument consists of three main parts shown in 3.1: (1) the environmental enclosure, containing the instrument computer, spectrometer and thermal electric cooler, (2) the telescope assembly mounted on the (3) 2-axis positioner capable of 180 ^{o} zenith and 360 ^{o} azimuthal rotations.

Figure 3.1: Pandora Ground-Based Spectrometer: (a) electronics box and the spectrometer; (b) 2-axis positioner with the telescope assembly; (c) deployment example on top of an EPA trailer [10].

The telescope assembly collects solar light with a field of view of 1.5 ^{o} (sky) and 2.6 ^{o} (direct sun). Bore being focused on the fiber (multi-mode, single core, 400 μm diameter) the light passes through two filter wheels. The fiber optics cable routs the light into the AvaSpec-ULS2048x64 spectrometer covering 270-530 nm wavelength region with 0.6 nm full width at half maximum spectral resolution (5 pixel sampling). The spectrometer is in a controlled environmental enclosure capable of maintaining temperature to $\pm 1^oC$.

Spinei at al. showed that the Pandora instruments generate HCHO within their telescope assembly due to the Delrin plastic off-gassing as a function of temperature (Delrin components

are being replaced since summer 2019) [22]. Internal to the instrument HCHO "contributes" to the atmospheric measurements from direct sun DOAS technique, significantly impacting the measurement accuracy. Data collected during past field campaigns from 2016 to summer 2019. Considering that HCHO measurements using other techniques are relatively rare due to the instrumental cost, Pandoras, in many cases, were the only instruments measuring HCHO during the major field campaigns.

3.3 Pandora participation in field campaigns

The Pandora instruments have participated in a number of field campaigns from 2016 to 2019 where information about HCHO presence was highly desirable. Three of these campaigns (KORUS-AQ, OWLETS, and LISTOS) included direct sun measurements with internally generated HCHO. The Korea-United States Air Quality Study (KORUS-AQ) took place during the months May-June of 2016. Pandora measurements during this campaign were made at multiple locations but for testing purposes in this study we use only one location: the megacity area of Olympic Park (37.5232°N; 27.1260°E; 26m a.s.l.) [21]. Measurements were made by both ground-based instruments including Pandora, as well as, airborne in-situ measurements made aboard NASA DC-8 research aircraft [21]. These measurements are meant to help address the need to monitor and understand air quality as the population grows and industrial and energy needs increase [2].

The Ozone Water-Land Environment Transitional Study (OWLETS) took place during the months July-August of 2017. Measurements were made at two research locations with six sites total in the Tidewater region of the Chesapeake Bay [23]. One site located directly over the Chesapeake Bay Bridge Tunnel with the other located over land at NASA's Langley Research Center. The purpose of this campaign was to characterized fundamental atmospheric processes occurring at the water-land interface [7]. Using forecasts provided by NOAA,

NASA, VA DEQ, the Maryland Department of the Environment, and other state agencies, OWLETS made intensive study of pollutant transport within the Chesapeake Bay watershed [23]. Collaboration and participation during this campaign included Federal and state agencies such as NASA, EPA, Maryland Department of the Environment and the Virginia Department of Environmental Quality amongst others [23].

The Long Island Sound Tropospheric Ozone Study (LISTOS) occurred during the months June-September of 2018. Partners in this campaign included a number of federal and state agencies including NASA, NOAA, EPA, New Jersey Department of Environmental Protection, New York State Department of Environmental Conservation and the Connecticut Department of Energy and Environment Protection amongst others [12]. Measurements included sensors for carbon monoxide, ground-based chemistry instruments for various atmospheric constituents, celiometers and spectrometers for evaluation an validation of satellite based instruments [12].

HCHO data collected by Pandoras during these campaigns was affected by the use of POM-H Delrin® parts now known to off-gas HCHO located within the telescope assembly causing an increase in HCHO seen in the measurement. However, it can be corrected if the internal to telescope assembly temperature is known and if internal HCHO production amplitude can be estimated which will be discussed in the proceeding sections.

Chapter 4

Formaldehyde offgasing from POM-H Delrin® plastic

4.1 Polyoxymethylene use in the Pandora telescope assembly

The Pandora head senor used POM-H Delrin® in manufacturing filter wheels and baffle holder. Specifically, POM-H, Ensinger Hyde: black Delrin® ecetal120resin II150ebk602 procured from McMaster Carr, part numbers: 8575K145 and 8576K21 [22]. "Polyoxymethylene (POM) is a semi-crystalline polymeric material belonging to engineering thermoplastics because of its low friction and wear characteristics and its excellent balance of mechanical properties and chemical resistance to most solvents, chemicals and fuels at room temperature" [14]. As a thermoplastic, POM has a large variety of uses since it's commercialization in the 1960s with six major manufactures supplying about 70 percent of the worldwide production [14]. The trade names supplied by these manufacturers are identified as POM-C Hostaform® Celcon® supplied by Ticona GmbH, POM-C Duracon® Tepcon® supplied by Polyplastics Co., Ltd., POM-H Delrin® supplied by E.I. Du Pont de Nemour & co., POM-C Kepital® supplied by Korea Engineering Plastics, POM-C Ultraform® supplied by BASF SE, and POM-C Teystron® and POM-H Delrin® supplied by Asahi-DuPont POM Co., Ltd. [14].

POM-H is created through the polymerization of purified gaseous HCHO resulting in a poly-

mer with a crystalline granular structure with macro molecules that end with at least one unstable hydroxyl group and it is these groups that create thermal instability in the polymer [22]. Degradation of POM mostly occurs from depolymerization, auto-oxidation scission, degradation by secondary production of auto-oxidation scission, hydrolysis and acidolysis, photo-oxidation in the wavelength region 200-800 nm, and thermal degradation. Most of these processes lead to HCHO emission as a byproduct and due to the regular operation mechanisms of the Pandora instrument it is likely that multiple degradation processes contribute to the degradation of the POM-H components used in their construction [22].

4.2 HCHO generation inside the Pandora telescope assembly

Spinei et al. [22] studied HCHO generation and deposition inside the Pandora telescope assembly due to POM-H degradation as a function of temperature. The deterioration of POM-H leading to the generation of HCHO can be attributed to several processes during the lifetime of the Pandora telescope assembly. Due to this, four Pandora telescope assemblies of different ages were evaluated: Pandora 21 (2011), Pandora 46 (2015), Pandora 118 (2016) and Pandora 148 (2018) [22]. The temperature in the enclosure containing the Pandora telescope assembly was varied from 10 ^{o}C to 45-55 ^{o}C held at the upper end for 0.5 to 1 hour and brought back to 10 ^{o}C at rates of 3, 3.5, 5, 8, 8.2 ^{o}C/hr. These rates were chosen to reflect realistic atmospheric conditions and temperature ranges due to the fact that thermal degradation of POM-H is heating rate dependent [18].

The DOAS Principle was used to determine the differential column densities of HCHO, ΔS^{hs}_{HCHO}, along the telescope assembly length from the front window to the lens relative to the amount at the reference temperature T^{ref}_{hs}. Figure 4.1 shows that HCHO columns inside the four studied Pandora telescope assemblies can be described by an exponential function

(Equation 4.1) with a damping coefficient, b, of 0.0911. Exponential function amplitude, a, however varied between $0.0041DU$ and $0.049DU$ between the instruments (age independent) [22].

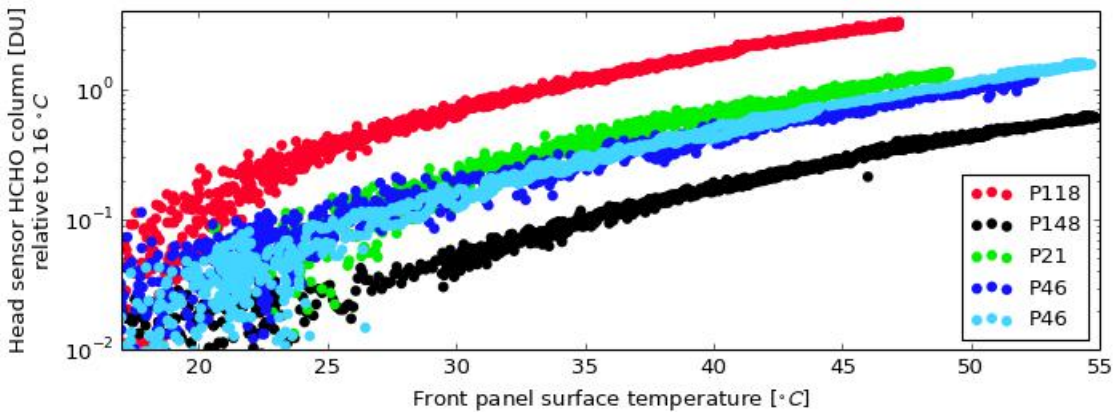

Figure 4.1: HCHO column densities present in four Pandora telescope assemblies as a function of temperature. Pandora 46 was tested twice with different rates of temperature change. Figure adopted from Spinei et al. [22].

$$\Delta S^{\text{hs}}_{\text{HCHO}}(\Delta T) = a \cdot \left[\exp(b \cdot T_{hs}) - \exp(b \cdot T^{ref}_{hs})\right] \tag{4.1}$$

This analysis suggests that amount of HCHO generated in Pandora telescope assembly can be estimated if internal temperature is known and if HCHO exponential generation amplitude is known. The following sections present proposed methodology to estimate both parameters from the Pandora direct sun measurements and ambient condition measurements (wind speed, wind direction, ambient temperature)

Chapter 5

Estimation of internally generated HCHO from direct sun measurements

DOAS fitting results from direct sun or multi-axis measurements ($\Delta S(\mu, \Delta T_{hs}, \Delta t)_{HCHO}$) accounting for internally generated HCHO ($S(T_{hs}, t)^{hs}_{HCHO}$) can be described by the following equation:

$$\underbrace{\Delta S(\mu, \Delta T_{hs}, \Delta t)_{HCHO}}_{measured} = \underbrace{\Delta S(\mu, \Delta t)_{HCHO}}_{atmospheric} + \underbrace{a \left[\exp(b \cdot T_{hs}) - \exp(b \cdot T^{ref}_{hs})\right]}_{telescope\ assembly} \tag{5.1}$$

Where a is an amplitude which is telescope assembly dependent and unknown for instruments that are not laboratory tested and b is a damping coefficient which is constant for all tested systems of approximately 0.0911. Due to this, the amplitude, a, must be derived from the data. A three-step approach is proposed and evaluated in the following sections to estimate HCHO columns from Pandora direct sun data. The first step determines the upper limit on the amplitude. The second step estimates the amplitude based on the HCHO columns measured at constant temperature bins. The third step estimates the amplitude based on the minimum Langley Extrapolation using iterative approach. Methodology is first tested on direct sun simulated $\Delta S(\mu, \Delta T_{hs}, \Delta t)_{HCHO}$ measurements.

Simulated $\Delta S(\mu, \Delta T_{hs}, \Delta t)_{HCHO}$ measurement description: Direct sun HCHO DOAS measurements are simulated based on the data collected during the KORUS-AQ campaign

at Olympic Park (NASA's KORUS-AQ data product website [4]). The available data include in situ HCHO surface concentration measurements from 8 May to 12 June 2016, Ceilometer backscatter data, meteorological data (ambient temperature, wind speed, wind direction) and Pandora direct sun measurements. Pandora telescope assemblies did not have internal temperature sensors until 2019. For the purpose of testing this method, a reasonable approximation for the internal telescope assembly temperature was used of 8^oC above the ambient temperature.

Spinei et al. [21] demonstrated that vertical column densities (C^{total} in Eq. 2.2) can be relatively accurately estimated from the in-situ surface measurements using mixing layer heights derived from Ceilometer backscatter data. Simulated direct sun S_{HCHO} calculation accounting for internal HCHO generation is done according to Eq. 5.2 where $C^{total}(t)$ is adopted from [21]. Exponential amplitude is assumed to be withing the measured in the laboratory range:

$$S(\lambda, t, T^t_{hs}) = C^{total}(t) \cdot AMF(\mu^t) + a \cdot \exp(b \cdot T^t_{hs}) \tag{5.2}$$

$S^{ref}(\lambda, \mu^{ref}, T^t_{hs})$ is calculated by taking the minimum of all data. This should correspond to the smallest AMF and C^{total} and most likely the lowest internal telescope assembly temperature T_{hs}. The final simulated measurement is calculated from Eq. 5.3

$$\Delta S(\lambda, \mu^t, \Delta T) = S(\lambda, t, T^t_{hs}) - S^{ref}(\lambda, \mu^{ref}, T^{ref}_{hs}) \tag{5.3}$$

Figure 5.1 shows ambient temperature measurements, $C^{total}_{HCHO}(t)$, direct sun AMF(t) and derived $S(\lambda, t, T^t_{hs})$. It is worth noting that the temperature dependent internal HCHO production depends on the ambient temperature with a peak in early-mid afternoon, while the actual measurements (ΔS and S) peak at higher solar zenith angles (AMF).

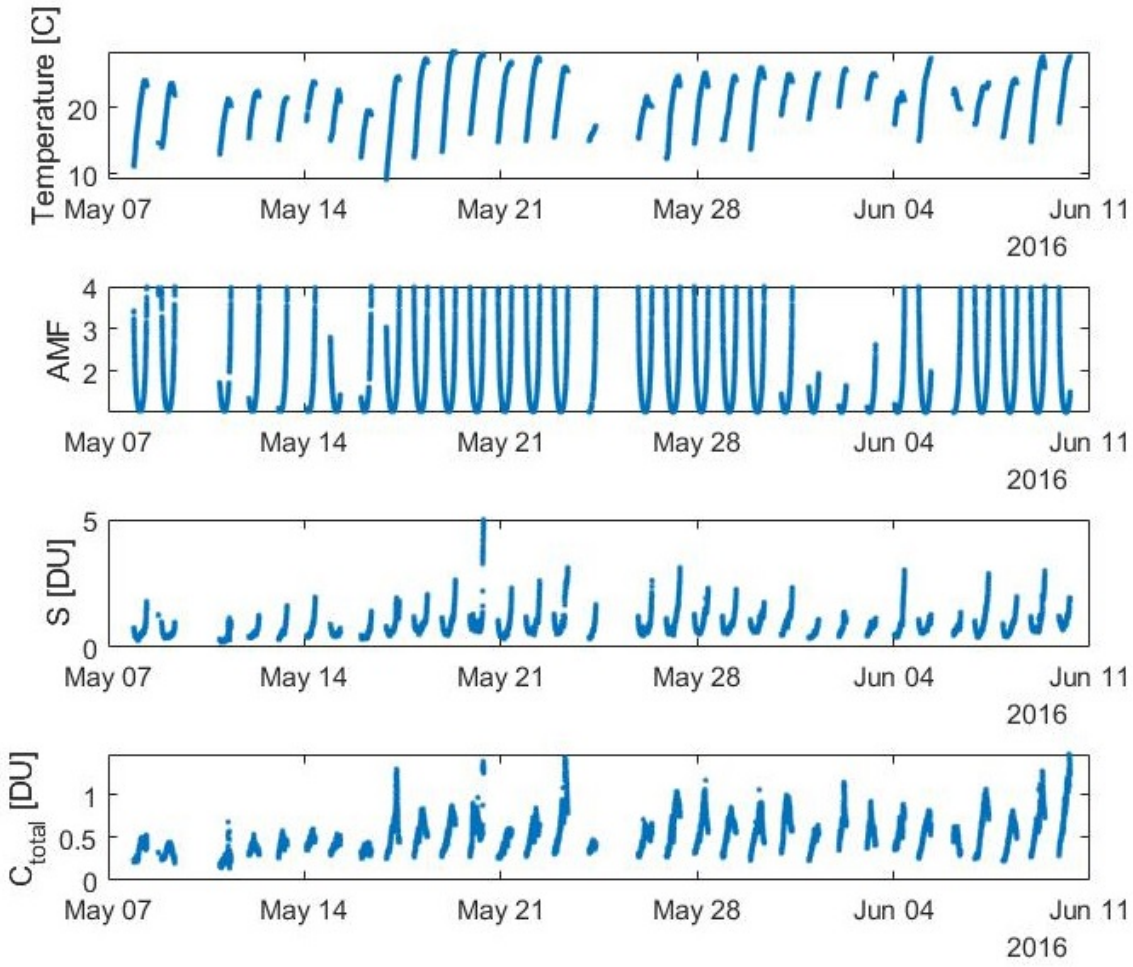

Figure 5.1: Simulated direct sun slant column densities calculated from (a) estimated total columns derived using in situ surface HCHO measurements and mixing layer heights; (b) estimated internal temperature inside the telescope assembly (ambient temperature + 8^oC; (c) direc air mass factors; and (d) exponential function amplitude $a = 0.0133DU$ and damping coefficient $b = 0.0911K^{-1}$ during KORUS-AQ 2016 campaign at Olympic Park site.

5.1 Step 1: estimation of the upper internal HCHO column production exponential amplitude

Internal HCHO column production exponential amplitude (slope) is estimated from Eq. 5.1 by performing linear regression analysis of the lowest percentile of the measured $\Delta S(\mu, \Delta t)_{HCHO}$

with respect to $\left[\exp(b \cdot T_{hs}) - \exp(b \cdot T_{hs}^{ref})\right]$. The result, however, can be impacted by the fact that atmospheric HCHO generation is also a function of the environmental conditions including temperature (e.g. isoprene, a major HCHO precursor, is emitted by deciduous trees as a function of temperature). Therefore, the resulting amplitude is the upper limit of the true amplitude that also potentially includes atmospheric HCHO temperature dependence. 2-percentile $\Delta S(\mu, \Delta t)_{HCHO}$ data are used in linear regression.

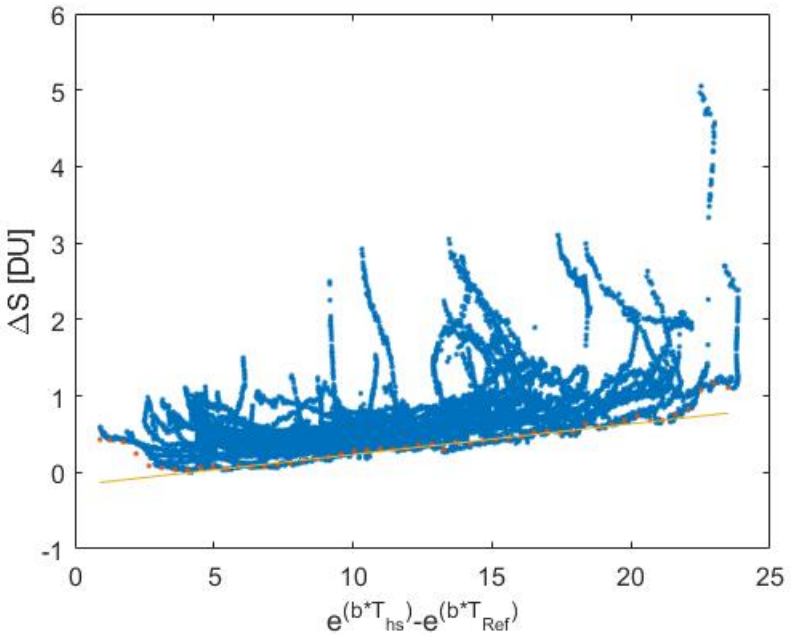

Figure 5.2: Demonstration of the 1st step to estimate upper limit of the exponential function amplitude for internally generated HCHO from the simulated direct sun differential slant column density (ΔS) and difference between the estimated internal temperature exponents where "true" $a = 0.0133DU$. A linear regression is applied to the 2-percentile data. Retrieved $a^{upper} = 0.0403DU$.

Step 1 was evaluated using various exponential function amplitudes for KORUS-AQ Olympic park direct sun simulated data. Figure 5.2 demonstrates this step (linear regression analysis) for $a = 0.0133DU$. The determined upper limit of the exponential function amplitude (slope) from this step is $a^{upper} = 0.0403DU$

5.2 Step 2: estimation of exponential production amplitude from data at different temperatures

The second step for retrieval of the instrument amplitude from direct sun data takes advantage of the fact that DOAS analysis cancels out HCHO generated by the POM-H parts if the same amount is present in the reference spectrum and the measured spectra. This condition is met when the spectra are measured at the same internal telescope assembly temperature. This is not realistic for an entire data set due to direct exposure to ambient conditions and therefor heat transfer processes. However, this can be realistic for a subset of data at some temperature T_1. Under these conditions a true atmospheric $S_{HCHO}(t_1)$ can be determined for a reference spectrum collected at time t_1 and head sensor T_{hs1} using Minimum Langley Extrapolation method. The same can be possible for a different temperature T_{hs2} ($\Delta T_{hs} = T_{hs2} - T_{hs1} > 2K$) and reference spectrum measured at time t_2. Then, the reference spectrum at t_1 and T_{hs1} can be used to analyse the spectrum at t_2 and T_{hs2}. Exponential function amplitude then can be determined according to Eq. 5.4

$$a = \frac{\Delta S(\mu, \Delta T_{hs}, \Delta t)_{HCHO} - [S_{HCHO}(t_2, T_{hs2}) - S_{HCHO}(t_1, T_{hs1})]}{\exp(b \cdot T_{hs2}) - \exp(b \cdot T_{hs1})} \tag{5.4}$$

The main limitation of this step is that MLE requires a significant amount of data at most AMF at the same temperature, which might not be available during short field campaigns.

To test this step KORUS-AQ data described above were used again. The data were grouped in 1^oC bins and MLE was applied to all ΔS data within each bin. Figure 5.3 shows the "best" pair results for $T_1 = 23^oC$ (top); $T_2 = 26^oC$ (bottom). The estimate amplitude using this step $a = 0.0144DU$ which is slightly overestimated (8%) comparing to the "true" amplitude of $0.0133DU$. Despite good agreement, Fig. 5.3 also shows that the available data in each

temperature bin are on the boarder of being insufficient for this type of analysis.

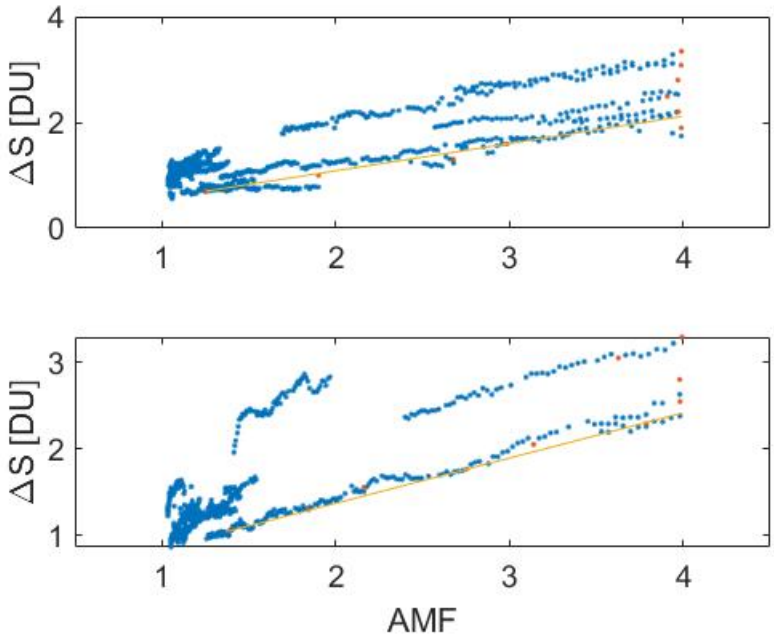

Figure 5.3: Demonstration of the 2nd step to estimate exponential internal HCHO production amplitude. Minimum Langley Extrapolation technique applied to the simulated differential slant column densities (see Fig. 5.1 for details) in $T_1 = 23 \pm 0.5°C$ (top); $T_2 = 26 \pm 0.5°C$ (bottom) bins.

5.3 Step 3: optimization of the MLE linear fit between the corrected ΔS and direct sun AMF

The slant column density depends on the vertical column density, air mass factor and the the production inside the telescope assembly with formulation shown in equation 5.2. While C_{HCHO}^{total} and the contribution from the telescope assembly both have some dependency on temperature, the AMF does not and this relationship may be exploited to obtain the amplitude corresponding to the instrument contribution alone.

The practical implementation of this step consists in iterative estimation of the exponential amplitude from the upper limit to zero in 1% steps and correction of the measured

$\Delta S(\mu, \Delta T_{hs}, \Delta t)_{HCHO}$ for the amount in the telescope assembly to determine the atmospheric only $\Delta S(\mu, \Delta t)_{HCHO}$ (Eq. 5.5). MLE analysis is then performed on the corrected data (atmospheric only estimation), where the quality of the linear fit is recorded as R^2. Considering that the temperature and AMF have opposite diurnal dependencies (increasing AMF at higher solar zenith angles when temperature is decreasing) quality of the MLE linear fit should improve when a more accurate amplitude is used for data correction.

$$\underbrace{\Delta S(\mu, \Delta t)_{HCHO}}_{atmospheric} = \underbrace{\Delta S(\mu, \Delta T_{hs}, \Delta t)_{HCHO}}_{measured} - \underbrace{a\left[\exp(b \cdot T_{hs}) - \exp(b \cdot T_{hs}^{ref})\right]}_{telescope\ assembly} \tag{5.5}$$

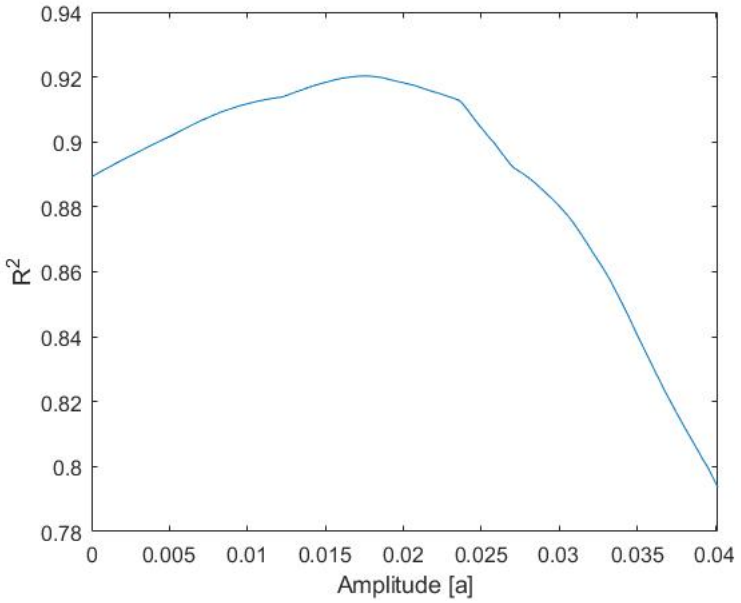

Figure 5.4: Demonstration of the 3rd step to estimate exponential internal HCHO production amplitude. Minimum Langley Extrapolation technique applied to the simulated differential slant column densities (see Fig. 5.1 for details) CORRECTED for POM-H HCHO offgassing using iterative amplitudes from 0.0433 to 0 DU. R^2 peak value occurs at 0.0175 DU, while the true a is 0.0133 DU

The biggest advantage of this step, compared to the 2nd step, is that all the measurements (at all temperatures) can be used to improve the statistics of the MLE analysis. This step also was tested using the KORUS-AQ simulated data described above and demonstrated for the

exponential function amplitude $a = 0.0133DU$. Figure 5.4 shows MLE linear fit R^2 values starting at $a^{upper} = 0.0433DU$ derived in the first step and decreasing by $\Delta a = 0.005DU$. The best MLE linear fit (expressed as R^2) is achieved at $a = 0.0175DU$ and is about 32% overestimation of the "true" $a = 0.0133DU$.

If there are enough data to perform step 2 and 3, an average of the two values can be considered the most accurate estimate of the exponential production amplitude.

Through this analysis it can be shown that given knowledge of the internal temperature of the Pandora telescope assembly a reasonable approximation for the HCHO generation due to off POM-H plastic gassing can be made from the Pandora data themselves. However, internal temperature data are not available for the Pandora instruments during KORUS-AQ (2016), OWLETS (2017,2018) and LISTOS (2018) campaigns. A methodology, then, must be developed for quantifying the internal temperature given the data that is available.

Chapter 6

Estimation of internal telescope assembly temperature

To provide an estimation of the internal telescope assembly temperature without the use of computationally expensive fluid dynamics modeling a steady state condition is assumed. Due to the relatively thin walls of the telescope assembly a lumped capacitance model can be assumed. The following heat transfer processes are responsible for internal telescope assembly temperature changes:

Forced convection due to wind can be represented by equation 6.1.

$$q_v = -h_v(\mu, ws) \cdot A \cdot (T_s - T_a) \tag{6.1}$$

Where, h_v is the convective heat transfer coefficient ($W/m^2/K$). This is dependent on wind speed (ws) and the telescope assembly's relative orientation (μ). T_s is the surface temperature and T_a is the ambient air temperature (K).

Radiant heat transfer to the telescope assembly can be defined by short wave absorption and long wave emission and absorption. Long wave heat transfer can be represented by

equation 6.2.

$$\begin{aligned} q_{lw} &= -\epsilon \cdot \sigma_{SB} \cdot A \cdot T_s^4 + \epsilon \cdot \sigma_{SB} \cdot 0.5 \cdot A \cdot T_a^4 + \epsilon \cdot \sigma_{SB} \cdot 0.5 \cdot A \cdot T_{sky}^4 \\ &= -\epsilon \cdot \sigma_{SB} \cdot A \cdot T_s^4 + \epsilon \cdot \sigma_{SB} \cdot A \cdot T_a^4 \cdot [(1 + \epsilon_{sky}) \cdot 0.5] \\ &= -\epsilon \cdot \sigma_{SB} \cdot A \cdot \left[T_s^4 - 0.5 \cdot (1 + \epsilon_{sky}) \cdot T_a^4\right] \end{aligned} \tag{6.2}$$

Where, the Stefan-Boltzmann constant, $\sigma_{SB} = 5.670{\times}10^{-8} W \cdot m^{-2} \cdot K^{-4}$. T_{sky} is the clear sky radiative temperature (K). ϵ_{sky} is sky emissivity which can be estimated as a function of dew point temperature T_{dp}. This relationship is represented by 6.3 and 6.4.

$$T_{sky} = T_a \cdot \epsilon_{sky}^{0.25}; \tag{6.3}$$

$$\epsilon_{sky} = 0.711 + 0.56 \cdot \frac{T_{dp}}{100} + 0.73 \cdot \left(\frac{T_{dp}}{100}\right)^2 \tag{6.4}$$

The short wave solar radiation can be represented by equation 6.5 and is the combination of the direct solar flux, solar radiance diffused by the sky and solar radiance reflected by the surrounding surfaces. The front panel of the telescope assembly is solar facing perpendicular to the direct solar radiance and is modeled by black or grey anodised aluminum properties. The back plate, also modeled by black or grey anodised aluminum, and the cylindrical sides of polished aluminum are exposed only to diffuse, scatted radiation during the operation.

$$q_{sw} = \left(I_{total}^{sun} \cdot \alpha_f \cdot (A_f - A_{fw}) + I_{total}^{sun} \cdot \alpha_{fw} \cdot A_{fw} + I_{diffuse}^{sun} \cdot [\alpha_s \cdot A_s + \alpha_b \cdot A_b]\right) \cdot h_{sw} \tag{6.5}$$

The energy generation inside the telescope assembly is represented by q_i. In addition, conduction between the telescope assembly and the tracker is represented by q_c. However, considering the small area of the connecting surface we ignore the contribution from con-

duction.

The overall steady state heat transfer equation can then be represented by equation 6.6.

$$h_v(\mu, ws) \cdot A \cdot (T_s - T_a) + \epsilon \cdot \sigma_{SB} \cdot A \cdot h_{lw} \cdot (T_s - T_a) = q_{sw} + q_i \tag{6.6}$$

To simplify the equation we define h_{lw} by equation 6.7 assuming $T_s = T_a + 8$[K]. This is based on previous experience with Pandora 148 in which the temperature inside the telescope assembly is about 1 to 15 °C higher than the ambient temperature depending on the wind conditions and ambient temperature.

$$h^*_{lw} = \frac{T_s^4 - T_a^4 \cdot 0.5 \cdot (1 + \epsilon_{sky})}{T_s - T_a} \approx \frac{(T_a + 8)^4 - T_a^4 \cdot 0.5 \cdot (1 + \epsilon_{sky})}{8} \tag{6.7}$$

Initial guess of the telescope assembly internal temperature is:

$$T^*_s = T_a + \frac{q_{sw} + q_i}{h_v(\mu, ws) \cdot A + \epsilon \cdot \sigma_{SB} \cdot A \cdot h^*_{lw}} \tag{6.8}$$

Recalculate h_{lw} with the initial estimation of T^*_s:

$$h_{lw} = \frac{T^{*4}_s - T_a^4 \cdot 0.5 \cdot (1 + \epsilon_{sky})}{T^*_s - T_a} \tag{6.9}$$

Recalculate the telescope assembly internal temperature according:

$$T_s = T_a + \frac{q_{sw} + q_i}{h_v(\mu, ws) \cdot A + \epsilon \cdot \sigma_{SB} \cdot A \cdot h_{lw}} \tag{6.10}$$

6.0.1 Accuracy of the internal telescope assembly temperature measurements.

Evaluating the HCHO emission of the POM-H parts in the Pandora telescope assembly requires knowledge of the accuracy of the internal temperature sensor used in the design of the Pandora telescope assembly. To quantify this value a comparison internal temperature measurements of four different Pandoras was conducted. These were Pandora 38, Pandora 57, Pandora 176 and Pandora 191. They were co-located on the roof of SciGlob, Inc. to ensure that the external conditions affecting the Pandora telescope temperatures were the same. Overlapping measurements occurred during 10-18 August 2020. The data were averaged over one minute intervals. Figure 6.1 depicts measured temperatures within four collocated Pandora instruments as well as the maximum range between them.

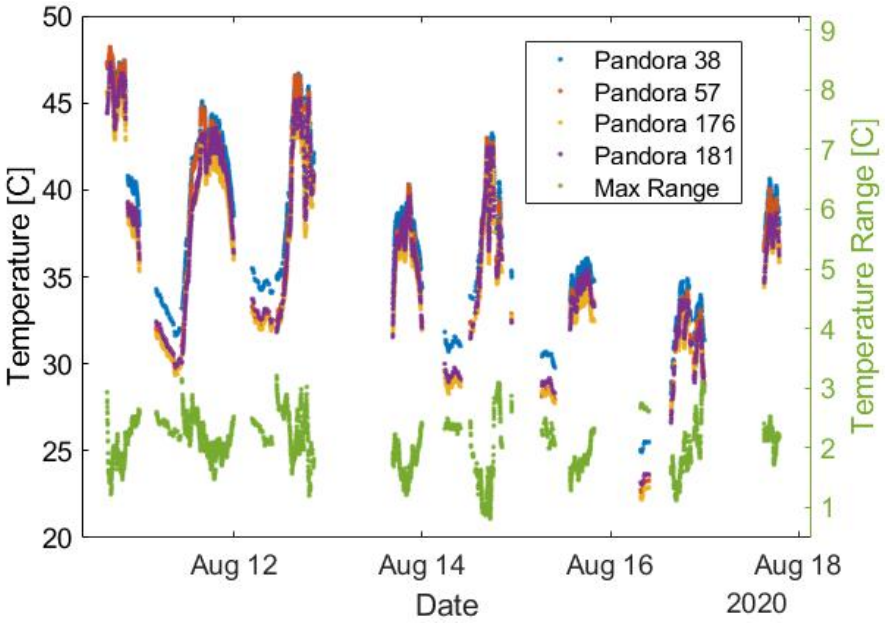

Figure 6.1: Internal temperature measurements from Pandora 28, 57, 176, 181 plotted with the maximum range respective to each data point.

The internal temperatures recorded during 10-18 August ranged between 22 and 48 ^oC with

a difference between the sensor measurements of of approximately 1 to 3 ^oC. Figure 6.2 shows a linear correlation between the median temperature and the temperature sensor measurements of Pandora 28, 57, 176, and 181. The linear regression analysis for Pandora 38 relative to the median is: R^2 of 0.983, an intercept of 3.015 and a slope of 0.959. For Pandora 57, it shows an R^2 of 0.986, an intercept of -1.02 and a slope of 1.039. For Pandora 176, it shows an R^2 of 0.996, an intercept of 0.265 and a slope of 0.979. For Pandora 181 it shows an R^2 of 0.999, an intercept of 0.363 and a slope of 0.992.

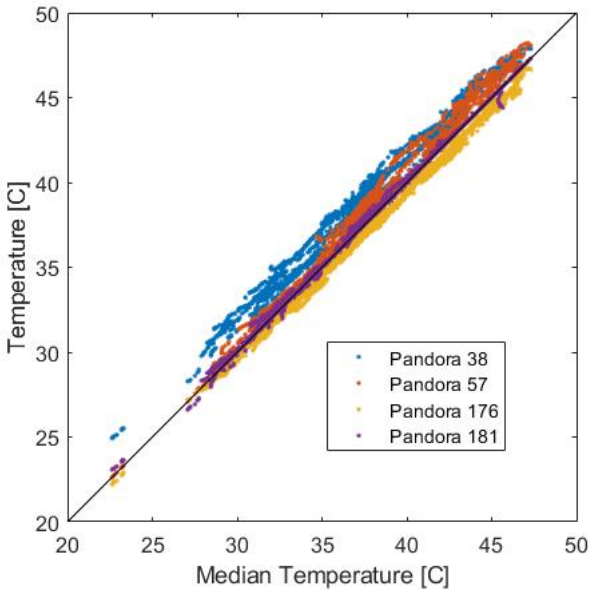

Figure 6.2: Internal temperature measurements from Pandora 28, 57, 176, 181 plotted against the median measurement between Pandora 57, 176, 181.

This suggests that the temperature sensors have high precision with an accuracy within $\pm 2^oC$ and 2%. The effect of potential inaccuracies in the derived temperatures will be compensated by the fact that exponential HCHO production amplitudes are derived from the Pandora data and temperatures.

6.0.2 Telescope assembly thermodynamics characterization

The heat transfer coefficient is dependent on the wind speed and orientation of the telescope assembly relative to the flow. To characterize this, testing of the instrument with the aid of a wind tunnel was conducted. The experiment was assisted by a Vaisala Weather Transmitter WXT520 to record wind speed and direction. Internal temperature measurements of the Pandora telescope assembly were made using a SparkFun temperature sensor. The temperature inside the telescope assembly is assumed to be spatially uniform and because of the relatively small thickness of outer walls the temperature difference is assumed to be very small as is consistent with a lumped system. We then assume that in the controlled environment of the wind tunnel, the radiative components are to be of negligible contribution. Then, in thermal equilibrium, the equation is reduced to…

$$Ah\Delta T + Q_{Gen} = 0 \tag{6.11}$$

Where, A is the surface area of the Pandora telescope assembly, h is the thermal transfer coefficient, ΔT is the temperature difference between the internal temperature and that of the air temperature and Q is the internal heat generation of the telescope assembly. The experiment was conducted at Virginia Polytechnic Institute and State University using the Aerospace and Ocean Engineering's Open Jet wind tunnel. The wind tunnel is powered by a centrifugal fan and capable of displacing air at a rate of 15 m3/s reaching a flow speed of approximately 30 m/s. The testing geometry and layout is shown in Figure 2.1.

The Pandora telescope assembly was mounted to a 2-axis tracker used in normal operations. The tracker mounted to a Celestron tripod, was secured in a position in which the telescope assembly is located at the center of the wind tunnel's exit flow. The weather station monitoring the wind speed and direction was placed off-center behind the telescope assembly

Figure 6.3: The wind tunnel setup for testing of Pandora instrument thermodynamic properties.

in a position which was unlikely to be affected by disturbances in the air flow caused by the presence of the telescope assembly. Testing was conducted at wind speeds of 0.4, 0.9, 2, 3.1, 4.4, 5.5, and 7.7 m/s to best represent the range in which operation typically takes place. For each trial, The RPM was set for the centrifugal fan corresponding to one of the air speeds. The internal temperature, air temperature and air speed were recorded and monitored for a time period long enough to allow for thermal equilibrium to be reached. Once change in temperature could no longer be observed the measurement was allowed to continue for an additional ten-minute period. The angle of the telescope assembly relative to the vertical position was then changed; adjusted in 20-degree increments of 0, 20, 40, 60 and 80 ^{o}. This process was timed, automated and repeated. A diagram showing the geometry of this procedure is shown below in Fig. 6.5.

As shown in the previous equation, the internal heat generation of the Pandora telescope

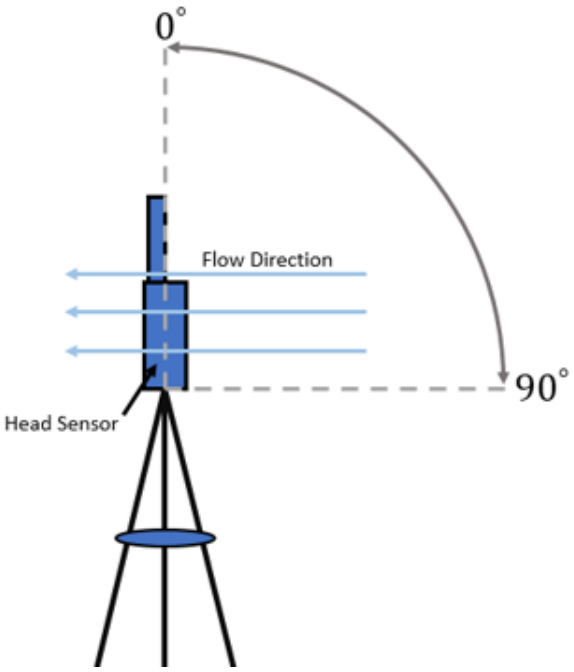

Figure 6.4: A diagram of the setup defining flow direction and angle of the Pandora telescope assembly relative to the air flow direction during testing.

assembly is required to create a model for the heat transfer coefficient at varying wind speeds and relative angles. For this purpose, internal heat generation was estimated through a series of measurements using FluxTeq's heat flux sensor. Heat generation local to the sensor is determined through the use of a thermopile constructed of material of known thermal conduction coefficient and thickness. This operates on the relationship shown below.

$$k = Qx/\Delta T \tag{6.12}$$

Where, k is the thermal conduction coefficient of the material, x is the thickness of the material, T is the temperature difference across the material and Q is the heat generation. FluxTeq's sensors were developed at Virginia Polytechnic Institute and State University with the oversight of Dr. Diller who co-founded FluxTeq and provided the sensor setup for measurement during this test. The Pandora telescope assembly was placed into the enclosure to prevent forced convection over its surface from external stimuli and held in

place by insulative foam to help prevent excess heat conduction through its mounting. The heat flux sensor and provided system for data acquisition self-calibrates with reference to a measurement of ambient temperature. The setup is shown in Figure 6.5.

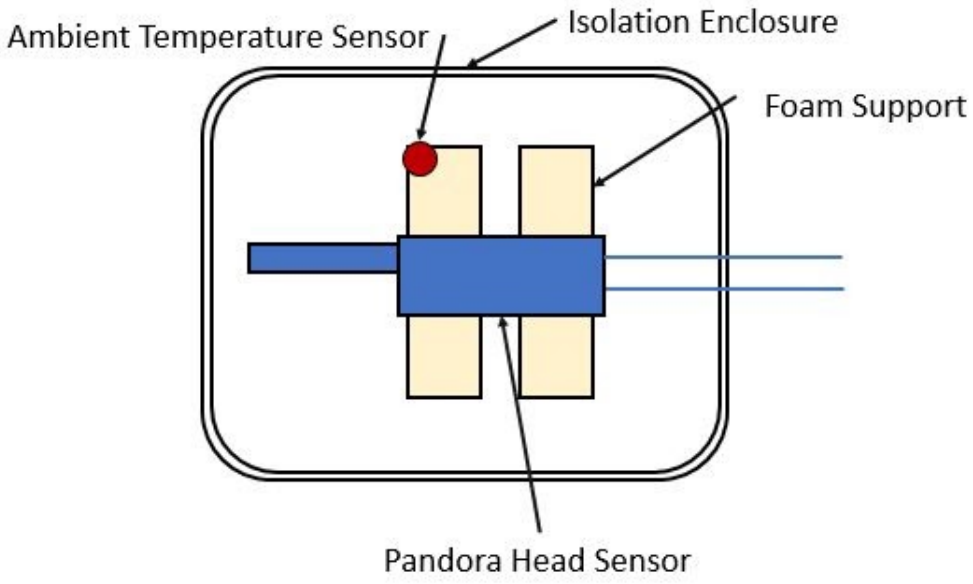

Figure 6.5: A diagram of the experimental setup used to measure heat flux.

The heat flux sensor took measurements in 16 locations along the body of the Pandora and at 1 location on both the solar and non-solar facing sides.

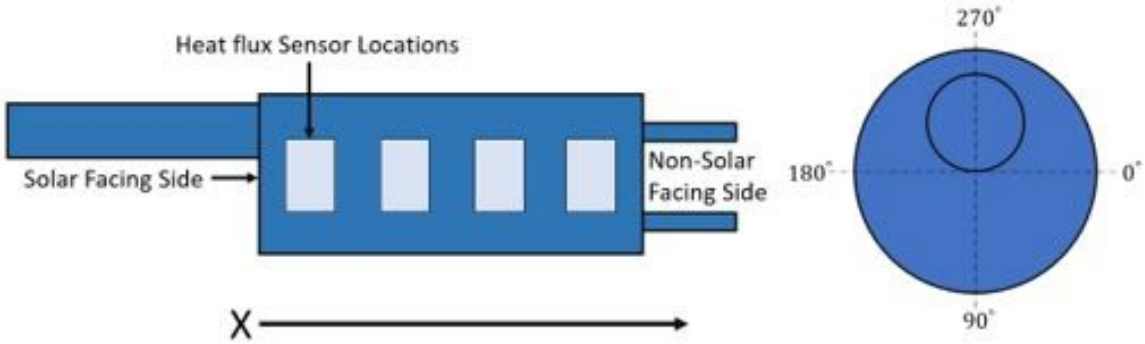

Figure 6.6: Diagram of the heat flux sensor locations on the telescope assembly body (Left). Solar Facing Side with a window (Right).

The heat flux sensor was placed in four locations separated by approximately 2 cm as shown

in Fig. 6.6. This was repeated 3 additional times rotating 90 degrees around the telescope assemblies central axis. The position of the telescope assembly was not altered during these measurements. The telescope assembly was made to simulate normal field operations. While monitoring the internal telescope assembly temperature, the rig was monitored, and sufficient time was allowed to reach an equilibrium state before any measurements using the heat flux sensor were taken. At each location 6 minutes of data was taken to provide a time-averaged value for that location.

Figure 6.7 shows the results of time-averaged heat flux measurements in (W/m^2). The x-axis are location numbers increasing in the x-axis shown in Figure 3, where 1 is the measurement taken on the solar facing side and 6 is that of the non-solar facing side.

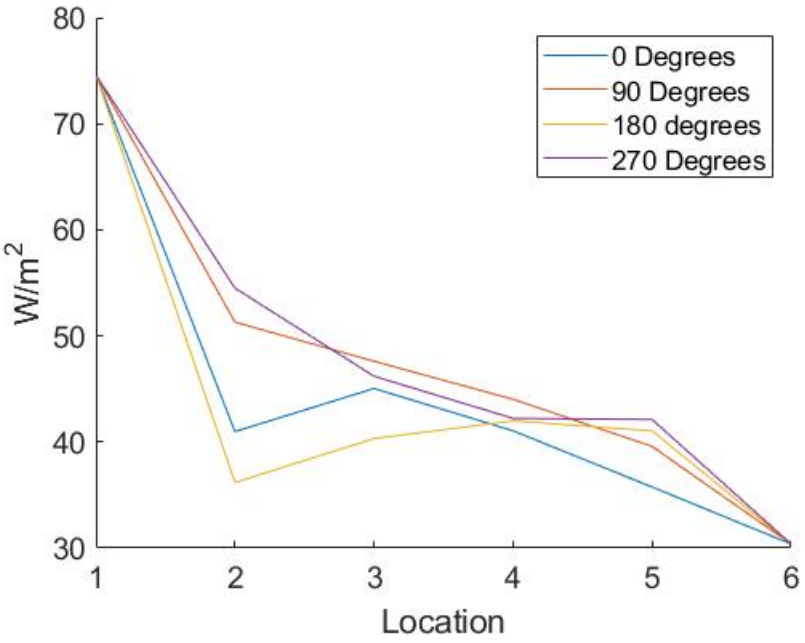

Figure 6.7: Time-averaged heat flux measured at locations increasing along the x-axis shown in 6.6.

6.1 Validation of the internal temperature estimation

The methodology described above for the estimation of the temperature internal to the Pandora telescope assembly was applied to data collected at Virginia Tech in Blacksburg, VA. The experiment was conducted from the rooftop of Whittemore Hall from June 29 to August 28 of 2019. Pandora 148 was used to collect data in conjuncture with pyranometer measurements attached directly to the telescope assembly for optimal positioning. Ambient temperature and wind conditions were measured through use of the Vaisala Weather Transmitter WXT520 positioned within a few feet of the instrument. The internal temperature for the telescope assembly was measured and is known as is the internal heat generation measured to be 2.43 W using the methods outlined in Section 6.0.2.

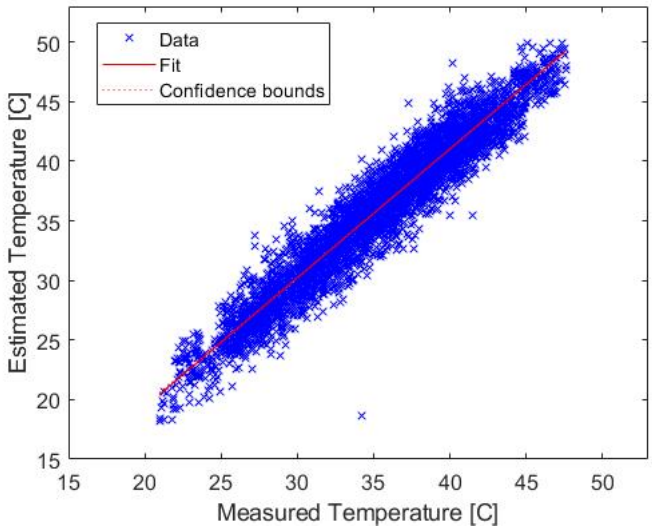

Figure 6.8: Estimated internal telescope assembly temperature for Pandora 148 during measurements in Blacksburg, VA in July - August 2018.

Figure 6.8 shows linear correlation between the estimated internal telescope assembly temperature and the measured temperature with $R^2 = 0.933$ and a slope of 1.005, suggesting a reasonable agreement between the estimated and measured internal temperature even assuming steady state conditions.

Chapter 7

Correction of direct sun HCHO Pandora measurements during KORUS-AQ

This section applies the proposed methodology for correction of the Pandora ΔS_{HCHO} measurements during the KORUS-AQ campaign for internally generated HCHO and presented by [21]. Ambient temperature data were not available for all days during the campaign at the Olympic Park. To provide an approximation of the temperature on the missing days, temperature data from the near by site of Taehwa was used and linear regression was performed against the temperature recorded at the Olympic Park site to provide formulation for the missing data. The methods for deriving the amplitude, a, described in Section 5, as well as, the method for determining the temperature internal to the Pandora telescope assembly described in Section 6 are applied to the data collected during KORUS-AQ. Figure 7.1 shows linear correlation analysis to determine the upper limit of the exponential function amplitude using step 1. The derived $a^{upper} = 0.0361DU$ This represents the amplitude accounting for temperature dependence of both instrument specific HCHO generation as well as atmospheric HCHO production. To calculate the amplitude the second step is applied to the data. Figure 7.2 shows that significantly fewer data points are available for the 2nd step from the actual data than from the simulated measurements. The derived amplitude $a = 0.0259DU$.

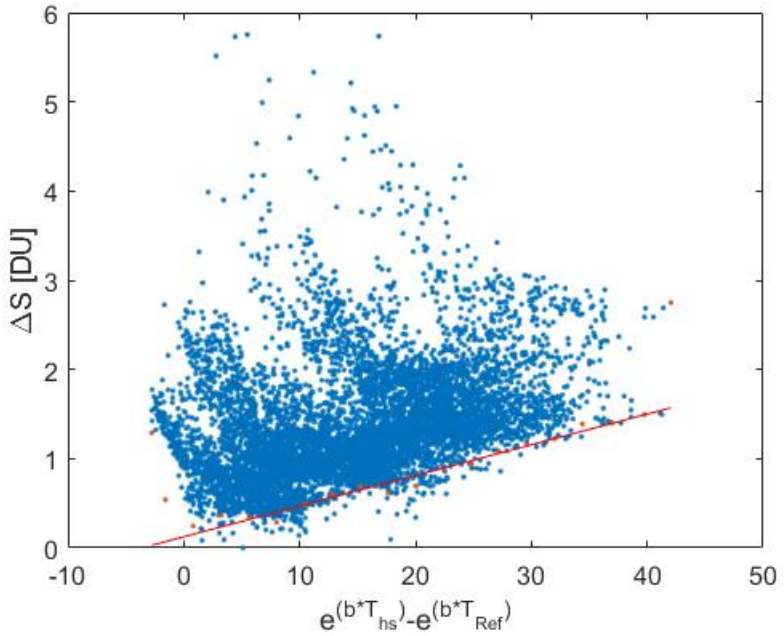

Figure 7.1: Determination of the upper limit of the HCHO internal exponential generation amplitude from Pandora 39 direct sun differential slant column densities (KORUS-AQ, May-June 2016): $a^{upper} = 0.03609DU$.

Using the upper amplitude limit determined in the first step as an initial starting point, the third step, an iterative MLE analysis of the fit between the corrected data and AMF, was performed and the results are shown in Fig. 7.3. The best R^2 value corresponds to the amplitude $a = 0.0208DU$. The mean value derived in steps 2 and 3 is used for actual Pandora HCHO data correction The results of this analysis are shown in Fig. 7.4. Total column measurements calculated from the in situ measurements aboard NASA DC-8 aircraft suggest that the corrected Pandora data agrees better with the DC-8 data than the original columns.

Figures 7.5 shows the HCHO relative column error of the original and corrected Pandora HCHO column measurements versus the DC-8 integrated columns.

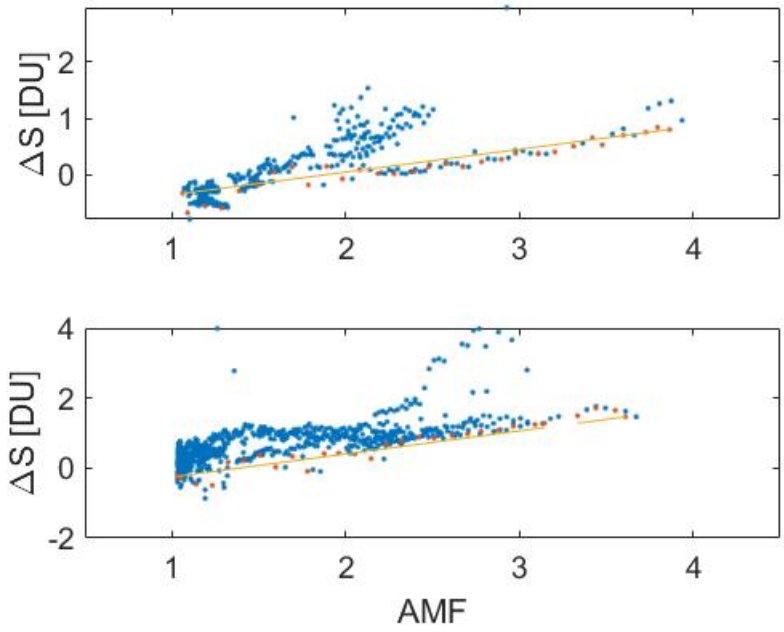

Figure 7.2: Minimum Langley Extrapolation technique applied to the differential slant column densities (see Fig. 5.1 for details) in $T_1 = 20 \pm 0.5°C$ (top); $T_2 = 27 \pm 0.5°C$ (bottom) bins. Derived a = 0.0259 DU.

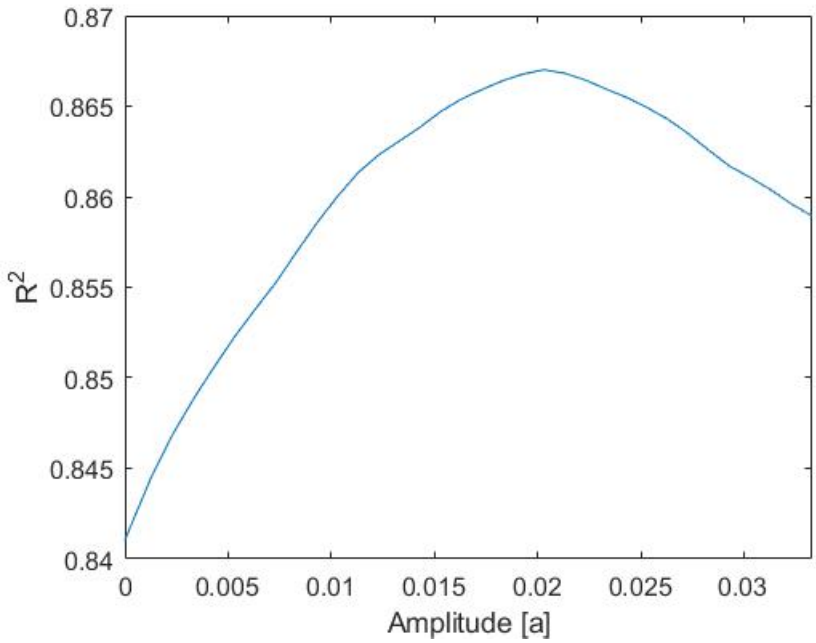

Figure 7.3: R^2 of the iterative MLE analysis performed on the corrected Pandora 39 differential slant column densities (see Fig. 5.1 for details) as a function of the exponential generation amplitude. The best fit corresponds to $a = 0.0208DU$.

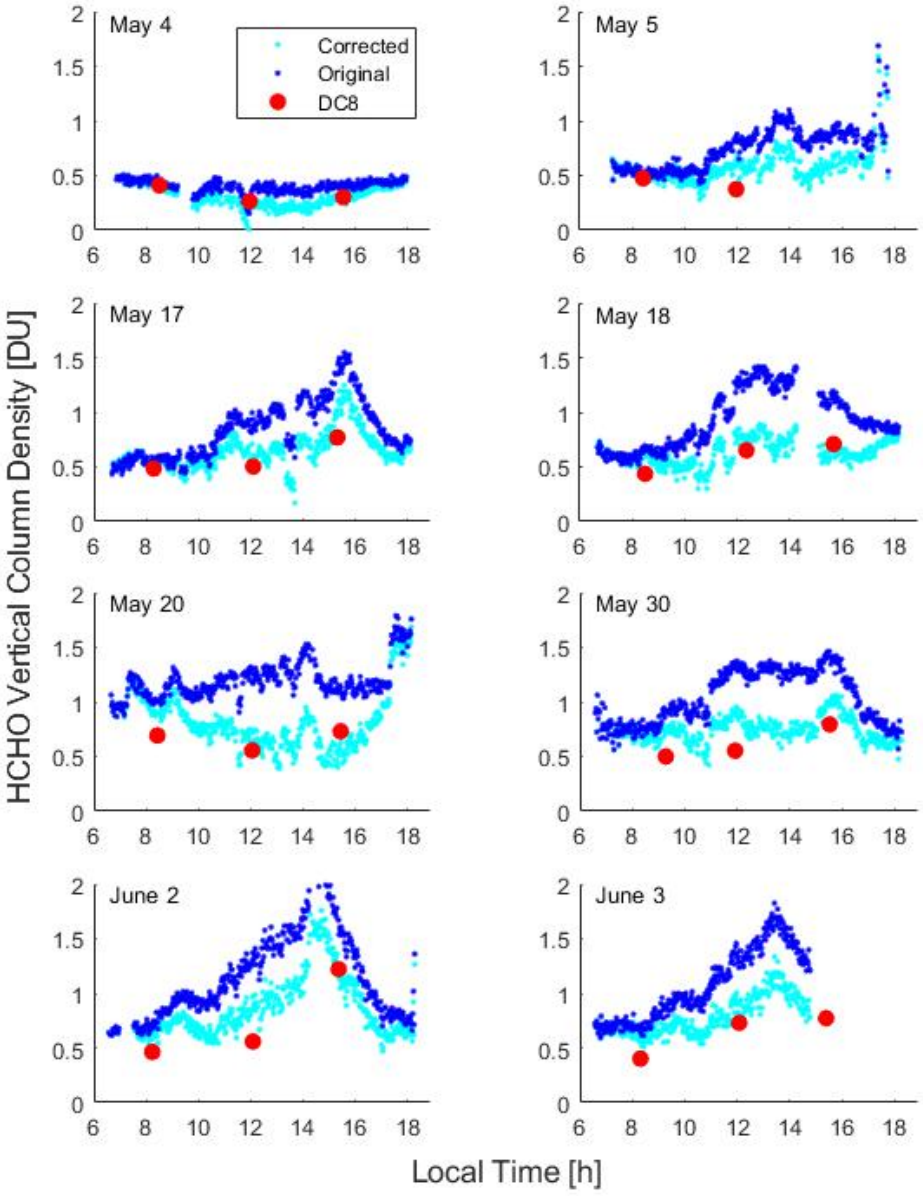

Figure 7.4: HCHO vertical columns measured by Pandora 39 in direct sun mode during KORUS-AQ over Olympic Park, South Korea (May-June 2016). Dark blue dots represent original data [21] including internally generated HCHO. Light blue are corrected data using methodology presented in this study. Red circles are DC-8 measured in situ integrated columns presented here for method evaluation.

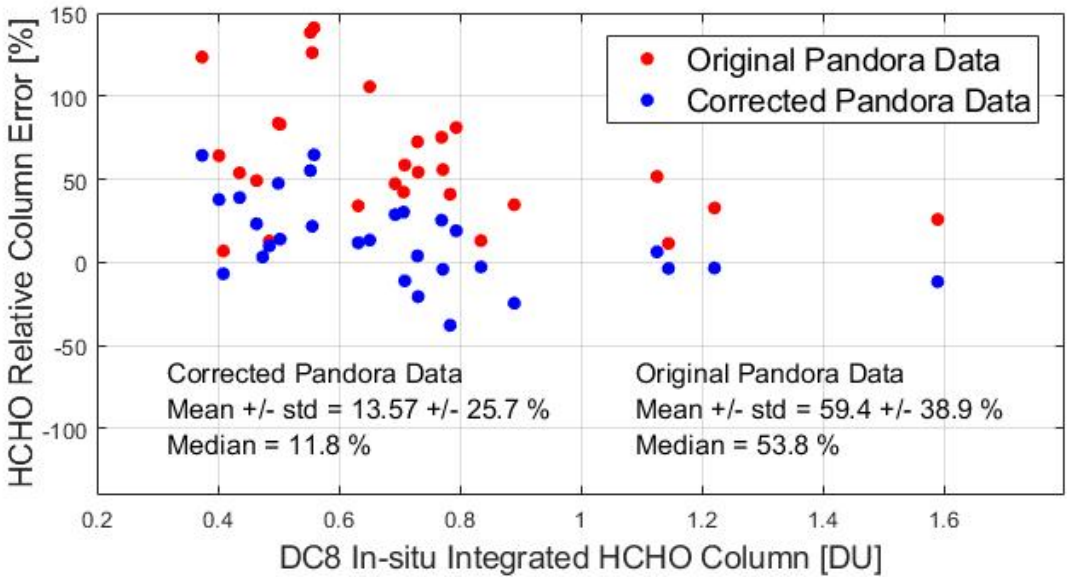

Figure 7.5: HCHO relative column error ($\frac{C_{Pandora}-C_{DC-8}}{C_{DC-8}}$) relative to DC8 in situ integrated HCHO column measured by Pandora 39 in direct sun mode during KORUS-AQ over Olympic Park, South Korea (May-June 2016).

Chapter 8

Discussion

The results in the previous section pertain to the KORUS-AQ field campaign over Olympic Park site and show that the methodology proposed in this thesis can be successfully used to improve the accuracy of the Pandora direct sun HCHO total columns during 2016 - 2019 short summer field campaigns. This conclusion was confirmed based on the simulated measurements and the comparison of the corrected Pandora HCHO columns with the integrated in-situ measurements made aboard NASA DC-8 aircraft.

The first step of the correction includes estimation of the internal telescope assembly temperature from the meteorological measurements collected at the site, including wind speed, wind direction, ambient temperature and shortwave solar flux. The temporal resolution of the meteorological data will impact the accuracy of the internal temperature estimation and as a result final HCHO correction. The current approach does not take into consideration non-steady state conditions which will impact the accuracy of temperature estimation. Future studies can look into using machine learning techniques to improve temperature estimation. On average the temperature agreement is good with the slope equal to 1 and intercept of 0.05^oC and $R^2 = 0.93$.

The second step of the correction includes estimation of the internal HCHO exponential generation amplitude knowing the internal telescope assembly temperature. The range of the laboratory measured amplitudes was found to be between 0.0041 and 0.049 DU. A 3-step method proposed here heavily relies on the data availability at different temperatures and air mass factors which can be challenging for a short field campaign. KORUS-AQ data set

was chosen due to its 1.5 months field campaign with mixed periods of cloudy and clear days that are representative of other field campaigns. The 1st step determines the upper limit of the amplitude and in theory should have enough data to conduct during a typical field campaign. The 2nd step uses data binned according to the telescope temperature and should have sufficient data at all air mass factors to perform MLE. This is a serious limitation for short field campaigns. Despite this, there were enough simulated data (assuming all days were cloud free), and the agreement between the "true" and estimated exponential amplitude was within 10%. Fewer actual Pandora measurements were available at this step due to clouds. Despite this the amplitude agreed with the 3rd step results within 25%. The 3rd step is an iterative application of MLE to the corrected HCHO differential slant column densities as a function of various exponential amplitudes. The amplitude is chosen based on the best MLE fit expressed as R^2. This step is not limited by the strict constrains of step 2, but still needs sufficient data for MLE. Evaluation of this step based on the simulated data suggests it is accurate within 30% in exponential amplitude estimation.

Finally, the corrected Pandora direct sun total HCHO column density measurements were compared to the integrated in-situ measurements made aboard DC-8 aircraft during the campaign shown in Fig. 7.4 and 7.5. The original HCHO columns measured by Pandora 39 in direct sun mode overestimated the DC-8 columns by $59.4 \pm 38.9\%$ (mean $\pm$ 1 std). The agreement between the data sets significantly improved after the Pandora HCHO data were corrected for internally generated HCHO. The corrected data agree with the DC-8 columns within $13.6 \pm 25.7\%$ (mean $\pm$ 1 std).

It is worth noting that the DOAS systematic fitting errors can be on the order of 35% depending on the choice of wavelength fitting window, Polynomial order, offset and the choice of molecular absorption cross sections.

Chapter 9

Conclusions

HCHO is the most abundant carbonyl in the atmosphere and is a key component for understanding oxidation in the atmospheric and by extension atmospheric health. Due to this fact, HCHO becomes a key component of study in field campaigns like LISTOS, OWLETS and KORUS-AQ. This study focuses on developing methodology to correct past Pandora direct sun measurements of HCHO. The design of the Pandora instrument used between 2016 and 2019 included parts made from POM-H plastic located internally to the telescope assembly. It has recently been shown that it off gases HCHO with a predictable dependence on temperature. The main goal of this thesis is to quantify the portion of the HCHO total column measured associated with the internal off gassing due to the POM-H parts. The methodology is evaluated using measurements collected during the KORUS-AQ campaign at the Olympic Park, South Korea (May - June 2016).

The proposed methodology for evaluating the off gassing of HCHO internally to the Pandora instrument consists in estimating internal telescope assembly temperature and calculating exponential generation amplitude. To evaluate temperature internal to the telescope assembly an extensive study was performed to analyze the thermodynamic properties of the Pandora telescope assembly derived from the empirical data collected through wind tunnel experimentation and heat flux measurements which was then applied to real data to test the validity of the method and were found to be in good agreement. Additionally, a three-step approach is developed to quantify the amplitude associated with the exponential temperature dependence of the HCHO production internal to the Pandora instrument for

instruments that have not been laboratory tested. These methodologies are applied to synthetic data derived from scaled in-situ measurements to verify their viability, found to be in good agreement, and are then applied to data collected by the KORUS-AQ field campaign producing HCHO total column densities that show substantial improvement in the agreement between the corrected measurements and those made by the aircraft. A comparison of the HCHO relative column error of the corrected and original data with respect to the DC8 aircraft measurements shows a substantial improvement from the correction evident in the mean error from approximately 59.4 to 12.57 %. It is then a recommendation that future work may include the quantification of the internally produced HCHO with respect to the other field campaigns with used the Pandora instrument containing POM-H parts utilizing similar methodology.

Bibliography

[1] IARC monographs on the evaluation of carcinogenic risks to humans, volume 88, formaldehyde, 2-butoxyethanol and 1-tert-butoxypropan-2-ol: this publication represents the views and expert opinions of an IARC working group on the evaluation of carcinogenic risks to humans, which met in lyon, 2 - 9 june 2004. Meeting Name: Meeting. IARC Working Group on the Evaluation of Carcinogenic Risks to Humans OCLC: 255440807.

[2] KORUS-AQ, . URL https://espo.nasa.gov/korus-aq/content/KORUS-AQ.

[3] Mobile-source air toxics: A critical review of the literature on exposure and health effects, .

[4] NASA airborne science data for atmospheric composition, . URL https://www-air.larc.nasa.gov/cgi-bin/ArcView/korusaq.

[5] Pandonia global network – reference measurements of atmospheric composition, . URL https://www.pandonia-global-network.org/.

[6] John C. Clausz, Bruce A. Maclntyre, Elizabeth S. Malone, and John M. Twelmeyer. Atmospheric formaldehyde levels in an academic laboratory. 61(4):A121. ISSN 0021-9584, 1938-1328. doi: 10.1021/ed061pA121. URL https://pubs.acs.org/doi/abs/10.1021/ed061pA121.

[7] Natasha Dacic, John T. Sullivan, K. Emma Knowland, Glenn M. Wolfe, Luke D. Oman, Timothy A. Berkoff, and Guillaume P. Gronoff. Evaluation of NASA's high-resolution global composition simulations: Understanding a pollution event in the chesapeake bay

during the summer 2017 OWLETS campaign. 222:117133. ISSN 13522310. doi: 10.1016/j.atmosenv.2019.117133. URL https://linkinghub.elsevier.com/retrieve/pii/S1352231019307721.

[8] I. De Smedt, T. Stavrakou, F. Hendrick, T. Danckaert, T. Vlemmix, G. Pinardi, N. Theys, C. Lerot, C. Gielen, C. Vigouroux, C. Hermans, C. Fayt, P. Veefkind, J.-F. Müller, and M. Van Roozendael. Diurnal, seasonal and long-term variations of global formaldehyde columns inferred from combined OMI and GOME-2 observations. 15(21):12519–12545. ISSN 1680-7324. doi: 10.5194/acp-15-12519-2015. URL https://acp.copernicus.org/articles/15/12519/2015/.

[9] C. Hak, I. Pundt, S. Trick, C. Kern, U. Platt, J. Dommen, C. Ordóñez, A. S. H. Prévôt, W. Junkermann, C. Astorga-Lloréns, B. R. Larsen, J. Mellqvist, A. Strandberg, Y. Yu, B. Galle, J. Kleffmann, J. C. Lörzer, G. O. Braathen, and R. Volkamer. Intercomparison of four different in-situ techniques for ambient formaldehyde measurements in urban air. *Atmospheric Chemistry and Physics*, 5(11):2881–2900, November 2005. ISSN 1680-7324. doi: 10.5194/acp-5-2881-2005. URL http://www.atmos-chem-phys.net/5/2881/2005/.

[10] J. Szykman, R.J. Swap, B. Lefer, L. Valin, S.C. Lee, V. Fidoletov, X. Zhao, J. Davies, D. Williams, N. Abuhassan, L. Shalaby, A. Cede, M. Tiefengraber, M. Mueller, A. Kotsakis, F. Santos, and J. Robinson. Pandora connection in-situ and satellite monitoring in support of the canada u.s. air quality agreement.

[11] N. B. Jones, K. Riedel, W. Allan, S. Wood, P. I. Palmer, K. Chance, and J. Notholt. Long-term tropospheric formaldehyde concentrations deduced from ground-based fourier transform solar infrared measurements. 9(18):7131–7142. ISSN 1680-

7324. doi: 10.5194/acp-9-7131-2009. URL https://acp.copernicus.org/articles/9/7131/2009/.

[12] Ali Aknan : NASA LaRC. NASA airborne science data for atmospheric composition. URL https://www-air.larc.nasa.gov/missions/listos/index.html.

[13] D. J. Luecken, S. L. Napelenok, M. Strum, R. Scheffe, and S. Phillips. Sensitivity of ambient atmospheric formaldehyde and ozone to precursor species and source types across the united states. 52(8):4668–4675. ISSN 0013-936X, 1520-5851. doi: 10.1021/acs.est.7b05509. URL https://pubs.acs.org/doi/10.1021/acs.est.7b05509.

[14] Sigrid Luftl, Visakh P. M., and C. Sarathchandran, editors. *Polyoxymethylene handbook: structure, properties, applications and their nanocomposites*. John Wiley & Sons, Scrivener Publishing, Hoboken, New Jersey : Salem, MA, 2014. ISBN 9781118914427 9781118914434.

[15] R. V. Martin. Evaluation of GOME satellite measurements of tropospheric NO $_2$ and HCHO using regional data from aircraft campaigns in the southeastern United States. *Journal of Geophysical Research*, 109(D24):D24307, 2004. ISSN 0148-0227. doi: 10.1029/2004JD004869. URL http://doi.wiley.com/10.1029/2004JD004869.

[16] T. Nash. The colorimetric estimation of formaldehyde by means of the hantzsch reaction. 55(3):416–421. ISSN 0306-3283. doi: 10.1042/bj0550416. URL https://portlandpress.com/biochemj/article/55/3/416/48059/The-colorimetric-estimation-of-formaldehyde-by.

[17] E. Peters, F. Wittrock, K. Großmann, U. Frieß, A. Richter, and J. P. Burrows. Formaldehyde and nitrogen dioxide over the remote western pacific ocean: SCIAMACHY and GOME-2 validation using ship-based MAX-DOAS observations. 12

(22):11179–11197. ISSN 1680-7324. doi: 10.5194/acp-12-11179-2012. URL https://acp.copernicus.org/articles/12/11179/2012/.

[18] Kinga Pielichowska. Thermooxidative degradation of polyoxymethylene homo- and copolymer nanocomposites with hydroxyapatite: Kinetic and thermoanalytical study. *Thermochimica Acta*, 600:7–19, January 2015. ISSN 00406031. doi: 10.1016/j.tca.2014.11.016. URL https://linkinghub.elsevier.com/retrieve/pii/S0040603114005231.

[19] G. Pinardi, M. Van Roozendael, N. Abuhassan, C. Adams, A. Cede, K. Clémer, C. Fayt, U. Frieß, M. Gil, J. Herman, C. Hermans, F. Hendrick, H. Irie, A. Merlaud, M. Navarro Comas, E. Peters, A. J. M. Piters, O. Puentedura, A. Richter, A. Schönhardt, R. Shaiganfar, E. Spinei, K. Strong, H. Takashima, M. Vrekoussis, T. Wagner, F. Wittrock, and S. Yilmaz. MAX-DOAS formaldehyde slant column measurements during CINDI: intercomparison and analysis improvement. *Atmospheric Measurement Techniques*, 6(1):167–185, January 2013. ISSN 1867-8548. doi: 10.5194/amt-6-167-2013. URL https://amt.copernicus.org/articles/6/167/2013/.

[20] Ulrich Platt and J. Stutz. *Differential optical absorption spectroscopy: principles and applications*. Physics of Earth and space environments. Springer, Berlin, 2008. ISBN 9783540211938 9783540757764.

[21] Elena Spinei, Andrew Whitehill, Alan Fried, Martin Tiefengraber, Travis N. Knepp, Scott Herndon, Jay R. Herman, Moritz Müller, Nader Abuhassan, Alexander Cede, Dirk Richter, James Walega, James Crawford, James Szykman, Lukas Valin, David J. Williams, Russell Long, Robert J. Swap, Youngjae Lee, Nabil Nowak, and Brett Poche. The first evaluation of formaldehyde column observations by improved Pandora spectrometers during the KORUS-AQ field study. *Atmospheric Measurement Techniques*,

11(9):4943–4961, August 2018. ISSN 1867-8548. doi: 10.5194/amt-11-4943-2018. URL https://amt.copernicus.org/articles/11/4943/2018/.

[22] Elena Spinei, Martin Tiefengraber, Moritz Müller, Manuel Gebetsberger, Alexander Cede, Luke Valin, James Szykman, Andrew Whitehill, Alexander Kotsakis, Fernando Santos, Nader Abbuhasan, Xiaoyi Zhao, Vitali Fioletov, Sum Chi Lee, and Robert Swap. Effect of Polyoxymethylene (POM-H Delrin) offgassing within Pandora head sensor on direct sun and multi-axis formaldehyde column measurements in 2016–2019. preprint, Gases/Remote Sensing/Instruments and Platforms, August 2020. URL https://amt.copernicus.org/preprints/amt-2020-158/.

[23] John T. Sullivan, Timothy Berkoff, Guillaume Gronoff, Travis Knepp, Margaret Pippin, Danette Allen, Laurence Twigg, Robert Swap, Maria Tzortziou, Anne M. Thompson, Ryan M. Stauffer, Glenn M. Wolfe, James Flynn, Sally E. Pusede, Laura M. Judd, William Moore, Barry D. Baker, Jay Al-Saadi, and Thomas J. McGee. The ozone water–land environmental transition study: An innovative strategy for understanding chesapeake bay pollution events. 100(2):291–306. ISSN 0003-0007. doi: 10.1175/BAMS-D-18-0025.1. URL https://journals.ametsoc.org/bams/article/100/2/291/69189/The-Ozone-Water-Land-Environmental-Transition. Publisher: American Meteorological Society.

[24] Wei Tan, Cheng Liu, Shanshan Wang, Chengzhi Xing, Wenjing Su, Chengxin Zhang, Congzi Xia, Haoran Liu, Zhaonan Cai, and Jianguo Liu. Tropospheric NO₂, SO₂, and HCHO over the east china sea, using ship-based MAX-DOAS observations and comparison with OMI and OMPS satellite data. 18(20):15387–15402. ISSN 1680-7324. doi: 10.5194/acp-18-15387-2018. URL https://acp.copernicus.org/articles/18/15387/2018/.

[25] C. Vigouroux, F. Hendrick, T. Stavrakou, B. Dils, I. De Smedt, C. Hermans, A. Merlaud, F. Scolas, C. Senten, G. Vanhaelewyn, S. Fally, M. Carleer, J.-M. Metzger, J.-F. Müller, M. Van Roozendael, and M. De Mazière. Ground-based FTIR and MAX-DOAS observations of formaldehyde at Réunion Island and comparisons with satellite and model data. *Atmospheric Chemistry and Physics*, 9(24):9523–9544, December 2009. ISSN 1680-7324. doi: 10.5194/acp-9-9523-2009. URL https://acp.copernicus.org/articles/9/9523/2009/.

[26] Folkard Wittrock, Andreas Richter, Hilke Oetjen, John P. Burrows, Maria Kanakidou, Stelios Myriokefalitakis, Rainer Volkamer, Steffen Beirle, Ulrich Platt, and Thomas Wagner. Simultaneous global observations of glyoxal and formaldehyde from space. 33 (16):L16804. ISSN 0094-8276. doi: 10.1029/2006GL026310. URL http://doi.wiley.com/10.1029/2006GL026310.

[27] Lei Zhu, Gonzalo González Abad, Caroline R. Nowlan, Christopher Chan Miller, Kelly Chance, Eric C. Apel, Joshua P. DiGangi, Alan Fried, Thomas F. Hanisco, Rebecca S. Hornbrook, Lu Hu, Jennifer Kaiser, Frank N. Keutsch, Wade Permar, Jason M. St. Clair, and Glenn M. Wolfe. Validation of satellite formaldehyde (HCHO) retrievals using observations from 12 aircraft campaigns. URL https://acp.copernicus.org/preprints/acp-2019-1117/.

[28] Lei Zhu, Daniel J. Jacob, Patrick S. Kim, Jenny A. Fisher, Karen Yu, Katherine R. Travis, Loretta J. Mickley, Robert M. Yantosca, Melissa P. Sulprizio, Isabelle De Smedt, Gonzalo González Abad, Kelly Chance, Can Li, Richard Ferrare, Alan Fried, Johnathan W. Hair, Thomas F. Hanisco, Dirk Richter, Amy Jo Scarino, James Walega, Petter Weibring, and Glenn M. Wolfe. Observing atmospheric formaldehyde (HCHO) from space: validation and intercomparison of six retrievals from four satellites (OMI, GOME2A, GOME2B, OMPS) with SEAC4RS aircraft obser-

vations over the southeast US. *Atmospheric Chemistry and Physics*, 16(21):13477–13490, November 2016. ISSN 1680-7324. doi: 10.5194/acp-16-13477-2016. URL https://www.atmos-chem-phys.net/16/13477/2016/.